Unidirectionally biased Permalloy: A polarized-neutron-reflection experiment

S. S. P. Parkin and V. R. Deline
IBM Almaden Research Center, 650 Harry Road, San Jose, California 95120-6099

R. O. Hilleke and G. P. Felcher
Argonne National Laboratory, Argonne, Illinois 60439

(Received 12 February 1990)

The depth profile of the magnetization of an exchange-coupled Permalloy-$Fe_{50}Mn_{50}$ bilayer is determined nondestructively from polarized-neutron reflectometry. The interfacial exchange coupling between the ferromagnetic Permalloy layer and the antiferromagnetic $Fe_{50}Mn_{50}$ layer gives rise to an unusual unidirectional anisotropy of the Permalloy layer, whose magnitude is much smaller than would be expected from the bulk exchange constants of these materials. A variety of models have been proposed to account for this result, some of which require inhomogeneous magnetization distributions within the Permalloy layer or at the Permalloy-$Fe_{50}Mn_{50}$ interface. These experiments reveal that, for a structure of the form Si(111)/$Ni_{81}Fe_{19}$(400 Å)/$Fe_{50}Mn_{50}$(400 Å)/Ta(300 Å), the depth profile of the magnetization is uniform within experimental error. In particular, for fields sufficiently large to magnetize the Permalloy layer at one or other extreme of the hysteresis loop, the layer-by-layer profile of the magnetization is identical, ruling out the possibility of planar domain-wall formation in the Permalloy layer. The hysteresis loop is derived from polarized-neutron reflectometry data as a function of in-plane magnetic field and is the same as that found using conventional magnetometry. The actual layer thicknesses of the structure were separately determined by neutron reflectometry for the structure magnetized with the magnetic moment perpendicular to the neutron-scattering plane.

I. INTRODUCTION

The phenomenon of exchange biasing, namely the occurrence of a unidirectional anisotropy, has been extensively studied since the late 1950's in coupled ferromagnetic-antiferromagnetic (F-AF) systems, such as Co/CoO and in spin glasses.[1-3] Recently there has been renewed interest in this novel anisotropy mechanism in thin film F-AF structures, where it is possible to grow tailor made structures of known geometry.[4-12] The most striking manifestation of this anisotropy is an asymmetric magnetic hysteresis loop displaced from zero field by the exchange bias field, H_B. One system displaying this type of behavior is that comprising the ferromagnet, $Ni_{81}Fe_{19}$ and the antiferromagnet, Fe_xMn_{1-x} ($x \simeq 0.5$). Although this system has been extensively studied, many of its properties remain poorly understood.[4-11] In particular, the magnitude of the exchange anisotropy is about 100 times smaller than simple estimates based on reasonable values of exchange constants.[12,13]

Various mechanisms have been proposed to account for the unexpectedly low values of exchange anisotropy in the Ni-Fe/Fe-Mn system. Unfortunately, this is a complex materials system and indeed even the magnetic structure of Fe-Mn remains somewhat controversial. However, the fact that the magnitude of the exchange anisotropy found for film couples prepared by different researchers under different preparation conditions is so similar, strongly suggests an intrinsic mechanism for the reduced magnitude.[11-13] Possible mechanisms include domain-wall formation in one or other of the magnetic layers.[11] Other mechanisms consider the results of imperfections at the interface. For example, depending on the magnetic structure of the Fe-Mn layer, terraces at the interface or intrusions of the Ni-Fe into the Fe-Mn layer or vice versa would cause the averaged exchange anisotropy to be reduced. To explain why the effect is not averaged completely to zero, Malozemoff[13] has recently developed a random-field model related to the size of possible domains in the antiferromagnetic layer resulting from defects of whatever origin at the interface. In order to check the applicability of these models a more detailed knowledge of both the magnetic and atomic structure at the interface is clearly needed.

In this work we have attempted to study the profile of the magnetization in a buried exchange coupled Permalloy layer in a typical structure of this type using the recently developed technique of polarized neutron reflectometry (PNR).[14] In addition, PNR can probe possible deviations of the magnetization from the uniform state for various applied fields near those required to switch the magnetization. While this is an ambitious problem for PNR, these studies establish that PNR provides a unique nondestructive method to determine the profile of the magnetization of a magnetic layer buried deep within a more complicated structure. Previously we have used PNR to determine the magnetic profile of thin single-layer magnetic films.[15]

In the following section the preparation and structural characterization of the sample is presented. Section III

includes a brief description of the polarized neutron reflection technique. This section also contains the PNR results obtained in this study. Section IV contains details of the method used to analyze these data and Sec. V contains results of this analysis as applied to the sample used in these experiments.

II. SAMPLE CHARACTERIZATION

The sample was prepared in a Perkin-Elmer 500 rf sputtering system, with a base pressure of $\simeq 10^{-8}$ Torr in an argon plasma at 10^{-3} Torr. The sample was deposited onto a highly polished (111) single-crystal silicon substrate of dimensions, 15×50 mm^2. The sample comprised a trilayer structure nominally consisting of $Si/Ni_{81}Fe_{19}$(400 Å)/$Fe_{50}Mn_{50}$(400 Å)/Ta(300 Å). The deposition took place in a field of $\simeq 100$ Oe applied parallel to the long axis of the sample. The Ta layer was used to reduce the possibility of oxidation of the magnetic layers. The sample displayed a magnetic hysteresis loop typical of other samples prepared at the same time but deposited onto thinner Si(111) substrates. After magnetic training the loop was characterized by a bias field, $H_B = 15$ Oe and a coercive field, $H_c = 5$ Oe.

The composition and structure of the sample was analyzed in detail using a wide variety of techniques including, Rutherford backscattering analysis (RBS), secondary-ion mass spectrometry (SIMS), secondary neutral mass spectrometry (SNMS), Auger sputter depth profiling, x-ray fluorescence, and x-ray diffraction.

A. X-ray analysis

The structure of both the Ni-Fe and Fe-Mn layers was fcc. Both layers were highly textured with the ⟨111⟩ direction oriented perpendicular to the plane of the film. Analysis of x-ray fluorescence data gave thicknesses of 335±5 Å for the Ta layer, 420±20 Å for the Fe-Mn layer and 400±20 Å for the Ni-Fe layer. These thicknesses were derived by assuming densities for the various layers calculated from the appropriate proportions of the bulk elements (Ta: 16.6 g cm^{-3}, Mn: 7.42 g cm^{-3}, Fe: 7.86 g cm^{-3}, and Ni: 8.9 g cm^{-3}). This analysis also assumed the composition of the permalloy was $Ni_{81}Fe_{19}$ but gave the composition of the antiferromagnetic layer as $Fe_{46}Mn_{54}$. The composition of the Permalloy layer was confirmed from electron microprobe analysis of a film prepared under similar conditions from the same sputtering target.

B. Rutherford backscattering analysis

The Rutherford backscattering (RBS) analysis was carried out with a 2.2-MeV He^+ beam, incident normal to the sample surface. The spectrum was measured at a backscattering angle of 120° with an integrated charge of 36 μC. The energy of the backscattered He^+ ions is largely determined by two loss processes. The first process involves elastic collisions with atoms in the sample. This process is characterized by an energy loss that decreases with increasing mass of the target atom and a higher scattering cross section for higher mass elements. The second process involves energy losses resulting from electronic interactions as the He^+ ions travel through the sample before colliding with an atom and on exiting the sample after the collision with a consequent shift of the energy of the backscattered radiation. Thus an RBS spectrum contains information on which elements are present as well as their abundance and distribution. The RBS spectrum obtained from the Si/Ni-Fe/Fe-Mn/Ta sample is shown in Fig. 1. The peak at the highest channel number or equivalently highest backscattered energy arises from the topmost Ta layer. The area under this peak corresponds to an areal atomic density of 1.78×10^{17} Ta/cm^2, and assuming a bulk density of 5.55×10^{22} Ta/cm^3, gives a Ta layer thickness of about 320 Å. The second largest peak between channels 350 and 410 corresponds to the Fe-Mn and Ni-Fe layers but the difference in mass between these three elements is too small for them to be separated in the RBS spectrum. The signal from Si is observed below channel 280. In addition to these main features, there is also a much smaller peak at channel number 440. This peak clearly corresponds to some element with much higher mass than Mn, Ni, or Fe. Its position is consistent with the presence of a small amount of Ta (approximately 1% of the large Ta peak) at the Si/Ni-Fe interface. Indeed the presence of Ta at the Si/Ni-Fe interface was subsequently confirmed by SIMS analysis. No Ta was detected at the Si/N:-Fe interface.

C. Auger electron spectroscopy

Auger sputter depth profiles were obtained with the use of a Perkin Elmer PHI-600 Auger system at an electron energy of 3 keV and an electron beam current of 0.46 μ amps into an area a few thousand Å in diameter. A 2 keV Ar^+ ion beam was used for sputter depth profiling. Auger peak intensities from O(503 eV), Si(92 eV), Mn(542 eV), Fe(703 eV), Ni(848 eV), and Ta(179 eV)

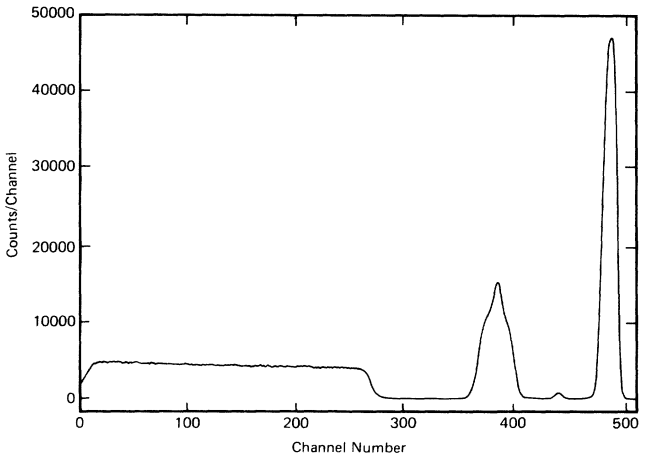

FIG. 1. RBS spectrum obtained from the sample of $Si/Ni_{81}Fe_{19}/Fe_{46}Mn_{54}/Ta$. The spectrum shows Ta on the surface (channels 471–500), Ta at the Si/Ni-Fe interface (430–443), overlapping Mn, Fe, and Ni signals (354–411), and the substrate Si (0–280).

were used for the depth profile. Published sensitivity factors were applied to construct the depth profiles shown in Fig. 2. The depth profile suggests that there is a concentration gradient across the Fe-Mn film with a composition of approximately $Fe_{50}Mn_{50}$ at the Fe-Mn/Ta interface and a Mn enriched composition of approximately $Fe_{45}Mn_{55}$ at the Ni-Fe/Fe-Mn interface. It is difficult to judge whether or not the interfaces at the Ta and Si surfaces are broader than that at the Ni-Fe/Fe-Mn interface as suggested by the data. This may simply be an experimental artifact, resulting from the smaller sputter-etch rates of the Si and Ta compared to Fe-Mn and Ni-Fe. The profiles of the interfaces are broadened by both the sputter process itself, resulting from sputter induced topography, and the Auger process that probes the escape depth of the Auger electrons (perhaps as much as 25 Å). The Auger data indicates no oxygen within the experimental detection limits. The increased oxygen Auger signal in the Fe-Mn layer shown in Fig. 2(b) may result from overlap of the Mn and O Auger peaks.

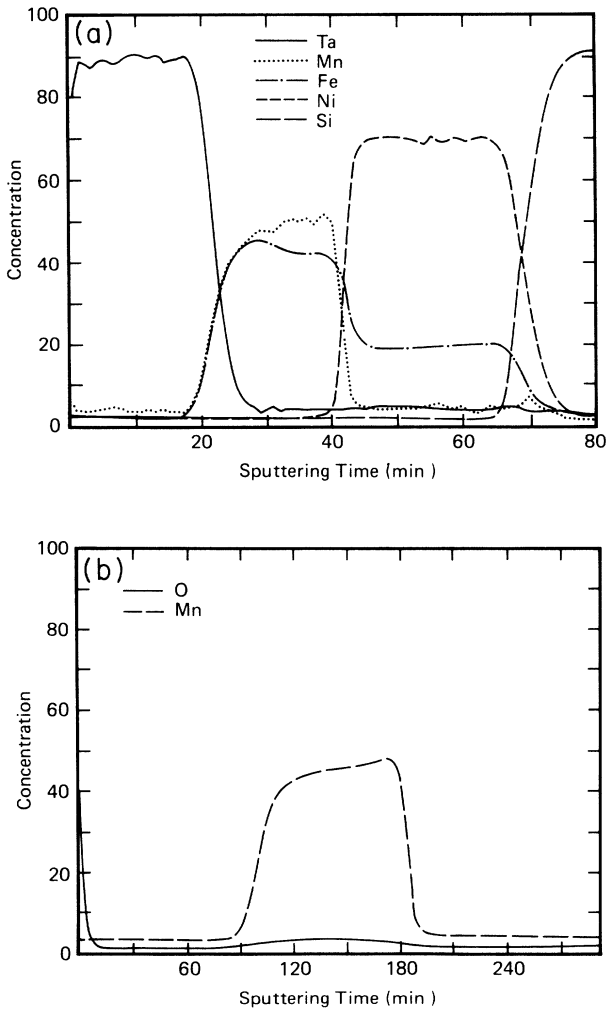

FIG. 2. AES depth profile of (a) Ta, Mn, Fe, Ni, and Si and (b) Mn and O obtained from the sample comprising $Si/Ni_{81}Fe_{19}/Fe_{46}Mn_{54}/Ta$. Note that part of the O signal from the $Fe_{46}Mn_{54}$ layer may be a result of overlap of the O and Mn peaks.

D. SIMS and SNMS

Secondary-ion mass spectrometry was carried out using an 8 keV O^{2+} ion beam and an oxygen back fill to increase secondary-ion yield and to reduce sputter-induced topography. In addition secondary neutral mass spectrometry was carried out to obtain improved depth resolution and better quantization resulting from the reduced dispersion in secondary-ion yields. SIMS data are shown in Fig. 3 and confirm the presence of a small amount of Ta at the Si/Ni-Fe interface together with the possible presence of a small amount of Mn. Moreover, a very small peak is found in the RBS spectrum at channel position 320 (Fig. 1) consistent with a trace amount of Mn at the Si interface. The SIMS depth profiles data suggest a constant composition ratio for both the Fe-Mn and Ni-Fe layers near the Ni-Fe/Fe-Mn interface in contrast to the Auger data. The peaks in the Mn and Fe SIMS depth profiles at the Fe-Mn/Ta interface and the Ni and Fe depth profiles at the Si/Ni-Fe interface are presumably artifacts resulting from variations in secondary ion yields possibly due to matrix effects. The increased yields at the Si/Ni-Fe interface may result from the presence of the native SiO_2. Indeed no such peaks are observed in the SNMS spectra. It is difficult to determine even the rela-

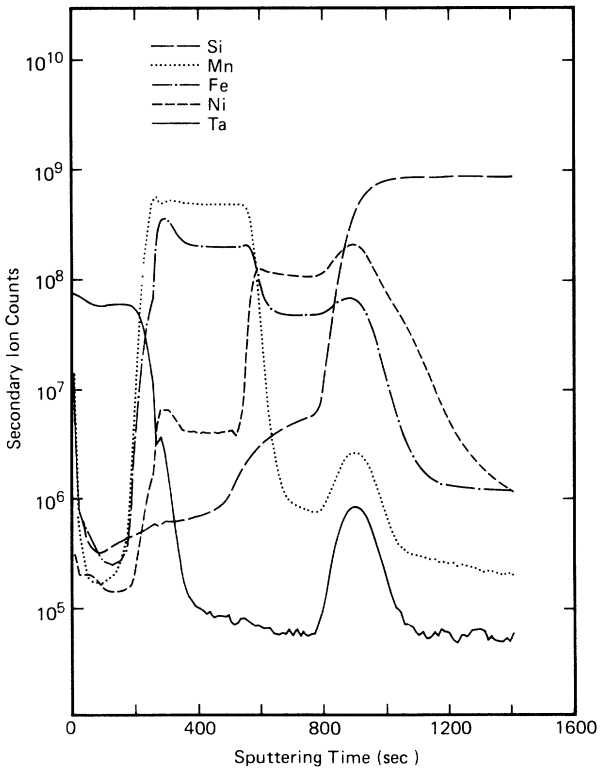

FIG. 3. SIMS depth profile of Si, Mn, Fe, Ni, and Ta obtained from the Si/Ni-Fe/Fe-Mn/Ta sample, using 8 keV O_2^+ bombardment with O_2 flood.

tive thicknesses of the Fe-Mn and Ni-Fe layers from either the Auger or SIMS data without detailed studies of appropriate calibration standards. It is not surprising that the data shown in Figs. 2 and 3 indicate different relative thickness ratios since different sputtering gases, energies and geometries were used. Both the SIMS and the SNMS data indicate trace amounts of Si throughout a significant fraction of the Ni-Fe layer.

III. POLARIZED NEUTRON REFLECTOMETRY

A. Experimental technique

The technique of polarized neutron reflectometry is described in detail elsewhere.[14] Briefly, a spin polarized beam of neutrons is reflected at grazing incidence θ from the surface of the specimen. The reflectivities for up and down spin neutrons, R^+ and R^- respectively, are measured at constant θ for a range of neutron wavelengths λ. The measured reflectivities, R^+, R^-, are optical transforms of the profiles of the nuclear and magnetic densities of the material as a function of the depth from the surface. These can be summarized by the following relations:

$$R^{\pm}(k_0) \leftrightarrow \left\{ \frac{b(z)}{V(z)} \pm \{c[B(z)-H]\} \right\}, \quad (1)$$

where k_0 is a physical variable that defines the component of the neutron momentum perpendicular to the surface and in vacuum, $k_0 = 2\pi(\sin\theta)/\lambda$, and where b/V is the average neutron scattering amplitude of the nuclei per unit volume at a depth z. In expression (1) B and H, the magnetic field applied to the system, have a common direction and lie in the scattering plane: The neutrons are polarized parallel (+) and antiparallel (−) to such a direction. The spin-dependent term is directly proportional to the magnetic induction B at the depth z, where the proportionality constant, $c = 2\pi\mu_n m/h^2$. For general systems and geometries, the dependence of the spin-dependent reflectivities on the nuclear and magnetic profiles can be written down by rigorous analytical expressions, but which contain k as an implicit variable.[16] Even more impractical are the analytical expressions for the inverse process, namely the determination of the nuclear and magnetic profiles[17] from $R^{\pm}(\lambda)$. These are found by attempting to construct the measured $R^{\pm}(\lambda)$ from trial profiles, as discussed in more detail in Sec. III.

The magnetic domain structure and the direction of the sample magnetization with respect to the neutron spin affect not only the magnitude of $R^{\pm}$ but also the extent of the depolarization of the reflected neutron beam.[14] The simplest cases to consider are those for which the orientation of the magnetization is the same throughout the thickness of the ferromagnetic layer. Several possible arrangements of this type are shown schematically in Fig. 4. The plus and minus signs refer to the relative polarizations of the neutron spin with respect to the applied magnetic field, **H**, which acts as a quantization axis for the polarized neutrons. When the F layer is magnetically saturated in the plane of the film along the direction of **H**, the neutrons remain polarized during the reflection process [Fig. 4(a)]. If the direction of the magnetization deviates from the quantization axis, the neutrons undergo a partial precession during the reflection process, so that the reflected beam is partially depolarized [Fig. 4(b)].

For applied fields within H_c of H_B the magnetization will not be saturated. If the sample is broken up into magnetic domains aligned either parallel or antiparallel to the applied field there will be no depolarization of the reflected beam. In this case, the reflectivities, $R^{\pm}$, will then be equal to an average of the sum of the reflectivities from the individual domains [Fig. 4(c)]. However this will only be true if the size of the domains is large in comparison with the coherence length of the neutrons, so that there is no interference between neutrons reflected from adjacent domains. Under these conditions it follows that the sum of the reflectivities for the two neutron states $[R^+(\lambda)+R^-(\lambda)]$ is independent of the domain structure and is identical to that for either of the saturated states obtained in large positive or negative fields. Finally, a very important result is that the magnetic term in Eq. (1) is sensitive to the direction of the applied magnetic field. In particular if H is applied perpendicular to the film and if H is sufficiently large to magnetize the sample in this

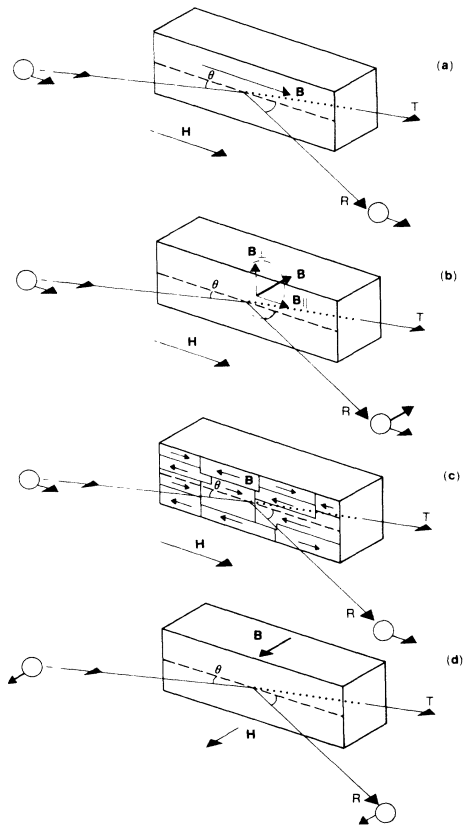

FIG. 4. Effects of the film magnetization on the neutron reflectivity and polarization. In configurations (a) and (b) the reflectivity is spin-dependent. For (c) the reflectivity is the average for that of the two neutron spin states while for configuration (d) the reflectivity is due only to nuclear interactions. In (b) the reflected beam is partially depolarized.

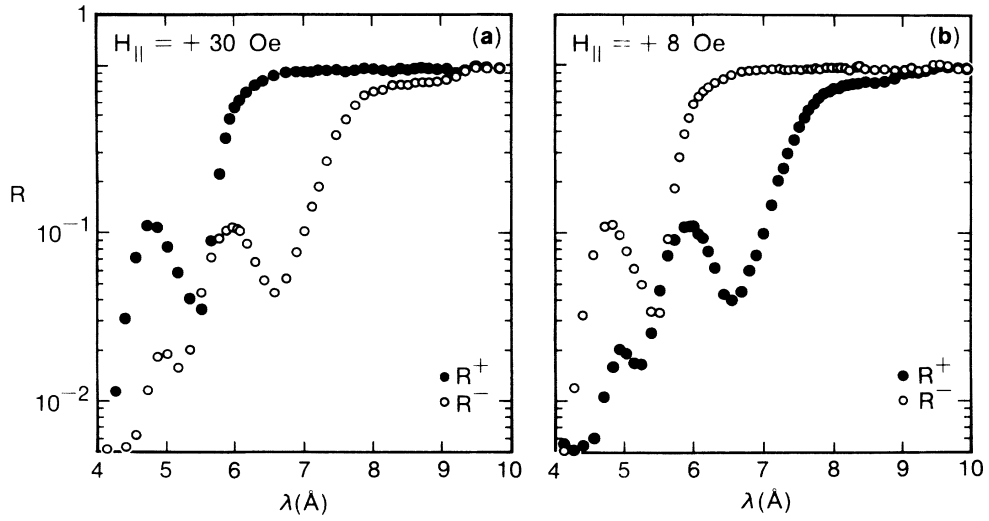

FIG. 5. Spin-dependent reflectivities vs neutron wavelength for in-plane applied fields of (a) 30 Oe and (b) 8 Oe.

direction, then since $B(z)-H$ is identically zero for all values of z the neutron reflectivities become spin independent. Thus in this geometry only the nuclear profile is measured [Fig. 4(d)].

B. Results

The polarized neutron reflectometry measurements were made at the Intense Pulsed Neutron Source at the Argonne National Laboratory. PNR data are presented in Figs. 5(a) and 5(b) for applied fields of 30 and 8 Oe, respectively. At these fields the magnetization of the sample is saturated at one or other extreme of the magnetic hysteresis loop. Large differences are clearly seen between the + and − neutron reflectivities which result from the magnetization of the Permalloy layer, and which obviously indicate that the sensitivity of this technique is sufficient to readily measure layers much less thick than that used here, namely $\simeq$400 Å. Note also that the + and − reflectivities are exactly reversed for the two different magnetic fields, corresponding to opposite states of the sample's magnetization with respect to the quantization field. This means that not only is the total magnetization of the sample the same for these two oppositely magnetized states, but that, more importantly, the profile of the magnetization through the film thickness is identical. An auxiliary measurement, which consisted in analyzing the polarization of the reflected beam, showed no depolarization for these cases.

The normalized difference of the two reflectivities, $P=(R^+-R^-)/(R^++R^-)$ is commonly called the polarization function. This quantity, integrated over a wide region of neutron wavelength, is proportional to the sample magnetization in a given magnetic field. Thus by measuring a series of reflectivity spectra at various fields and finding P as a function of H, a hysteresis loop is obtained, as shown in Fig. 6. This loop, as determined by PNR, was very similar to that directly measured using a vibrating sample magnetometer, showing that the assumption implicit in determining the PNR loop, that the magnetic profile is independent of field, is a reasonable one. Furthermore, no depolarization of the neutron beam was found even for intermediate fields near H_c, and, in all cases, the sum of the + and − reflectivities was identical to that obtained for the saturated states.

Thus, without any detailed analysis of the reflectivity spectra, a great deal can be inferred about the magnetic state of the Permalloy layer. In particular, the magnetic state of this layer is the same at either extreme of the hysteresis loop. At the transition, the layer breaks up into magnetic domains, each large compared to the neutron coherence length, and each with a magnetization aligned either parallel or antiparallel to the quantization axis. To obtain more information on the distribution of the magnetization within the Permalloy layer, the reflectivity spectra was analyzed in detail, using the procedure outlined in the following section.

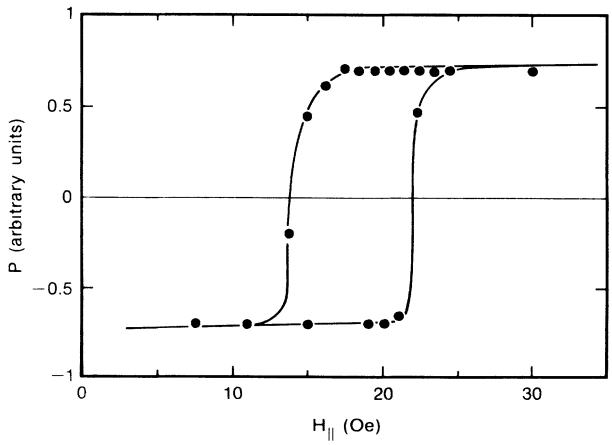

FIG. 6. Polarization function vs in-plane applied field.

IV. METHOD OF ANALYSIS

Methods to calculate the reflectivity from an arbitrary stack of sheets of different refractive index are well known.[17,18] The treatment given here offers a systematic approach to the analysis of the experimental reflectivities, giving some insight into the structure of the material studied. In the following discussion, for simplicity, the magnetic term in Eq. (1) is neglected. This term is trivially introduced by replacing b/V with $b/V \pm cB$.

The reflectivity is given by $R=|r_t|^2$, where r_t is the reflectance of the total system. Suppose that the system is made up from $n-1$ slabs, of thickness z_i, each characterized by a scattering amplitude per unit volume, $(b/V)_i$. The component of the neutron momentum normal to the surface, k_0, in vacuum becomes in layer i,

$$k_i=\sqrt{k_0^2-4\pi b_i/V} \tag{2}$$

and the reflectance at the boundary between the ith and the $(i+1)$th layer is given by

$$r_{i,i+1}=\frac{k_i-k_{i+1}}{k_i+k_{i+1}} . \tag{3}$$

These relations are sufficient to write down an expression for the total reflectance. To do so it is convenient to first express r_t explicitly only in terms of the reflectance $r_{n-1,n}$, at the final interface between the $(n-1)$th layer and the substrate, as follows:

$$r_t=r_{0,n}=\frac{r_{0,n-1}+r_{n-1,n}\exp(2ik_{n-1}z_{n-1})}{1+r_{0,n-1}r_{n-1,n}\exp(2ik_{n-1}z_{n-1})} . \tag{4}$$

Similarly, the reflectance of the topmost $n-2$ layers, $r_{0,n-1}$, can be expressed as

$$r_{0,n-1}=\frac{r_{0,n-2}+r_{n-2,n-1}\exp(2ik_{n-2}z_{n-2})}{1+r_{0,n-2}r_{n-2,n-1}\exp(2ik_{n-2}z_{n-2})} , \tag{5}$$

where only the reflection coefficient at the penultimate interface is explicitly included. This procedure can be continued until an expression for the very first layer is obtained. Obviously, the resulting expression is quite cumbersome. However, it takes a much simpler form for values of neutron momenta for which the reflectivity is weak, or where the neutron momentum is only weakly perturbed by the medium. Under these conditions we obtain the expression,

$$r_{0,n}k_0^2=\pi\sum_{i=1}^{n}\left[\left(\frac{b}{V}\right)_i-\left(\frac{b}{V}\right)_{i-1}\right]\exp\left[\sum_{i'=1}^{n-1}2ik_{i'}z_{i'}\right] , \tag{6}$$

which is quite similar to the expression for the structure factor of a crystalline cell as used in x-ray or neutron-scattering theory.[19] By analogy, $(b/V)_i-(b/V)_{i-1}$ takes the place of the atomic scattering amplitude. The phase factor, in this case, depends not simply on the position of the $i,i+1$ interface, as in conventional diffraction theory, but also on the path of the neutron beam through the preceding i layers which alters its momentum. The modulus of the square of the expression (6) gives the observed reflectivity:

$$\frac{1}{\pi^2}Rk_0^4=D+2\sum_{\substack{ij\\ i>j}}\left[\left(\frac{b}{V}\right)_i-\left(\frac{b}{V}\right)_{i-1}\right]\left[\left(\frac{b}{V}\right)_j-\left(\frac{b}{V}\right)_{j-1}\right]\cos\left[2\sum_{l=j-1}^{i-1}k_l z_l\right] \tag{7a}$$

and

$$D=\sum_i\left[\left(\frac{b}{V}\right)_i-\left(\frac{b}{V}\right)_{i-1}\right]^2 . \tag{7b}$$

The structure of Eq. (7) is interesting. In the case of a single reflecting surface, the reflectivity multiplied by k_0^4 is a constant. For a more complicated system, Rk_0^4 oscillates about this constant value such that as the range of k_0, for which observations are made, is expanded more and more details about the system can be obtained. Borrowing definitions used in conventional scattering theory (in the first Born approximation) a spatial resolution, dz is obtained by extending the range of measurements to a value of k_0 such that k_0 satisfies $k_0 dz=\pi$. This rule is valid only when applied to a range of k_0 large compared with the momentum at which there is total reflection.

The right-hand side of Eq. (7a) contains a constant term plus $n(n-1)/2$ oscillating terms for $(n-1)$ layers. The analysis rapidly becomes more complicated as the number of layers is increased. Each oscillating term represents a layer, defined by a front and back interface. Its amplitude depends solely on the product of the reflectances at the two boundaries. The argument of each cosine function is proportional to the layer thickness such that the interference function oscillates more rapidly the thicker the layer. However, the function is not exactly periodic with k_0 except in the limit of large k_0 values.

In order to understand more clearly which quantities can be derived from knowledge of the maxima and minima of the interference function,[20] consider the simplest case of reflection from a single layer on a substrate. In this case, Eq. (7) contains only one cosine term and its argument depends only on one value of k_i, which is related to the refractive index of the layer via Eq. (2). Thus it is clear that both the thickness of the layer and the scattering potential of the layer can be found from the positions of the minima in k_0. Note that a more accurate expres-

sion can be derived for a single layer than the approximate expression given in Eq. (7). The exact formula is

$$R_{0,2}=\frac{r_{0,1}^2+r_{1,2}^2+2r_{0,1}r_{1,2}\cos(2k_1z_1)}{1+r_{0,1}^2r_{1,2}^2+2r_{0,1}r_{1,2}\cos(2k_1z_1)} . \quad (8)$$

The presence of the term in the denominator does not shift the minima of the cosine function but makes them considerably sharper.

The preceding discussion suggests the most appropriate procedure to analyze the experimental results is to plot $k_0^4R(k_0)$ with respect to k_0. Assuming that the number of layers, their approximate thicknesses and the approximate boundary reflectances are known, then the layers can be identified from the position of the interference minima, beginning with the strongest terms. An iterative procedure then follows in which detailed calculations of $k_0^4R(k_0)$ are compared with experiment.

In the preceding discussion we have considered systems comprising a sequence of layers, each with a well-defined refractive index. Even if the refractive index varies continuously throughout the film thickness, this case can be adequately approximated by a sufficiently large number of layers. However there are a few profiles for which there exist exact solutions. One of these is relevant to the physically important case in which the interface between successive layers is laterally rough perhaps resulting from interdiffusion or the growth mode of the layers. The refractive index exhibits fluctuations along the interface which we shall assume are random. The interface then has an effective thickness, $\langle Z^2\rangle^{1/2}$. It has previously been shown that the reflectance of such a rough interface is related to that of the reflectance of the abrupt interface by a Debye-Waller factor, as follows,[21]

$$(r_{i,i+1})_{\text{rough}}=(r_{i,i+1})_{\text{sharp}}\exp(-k_ik_{i+1}\langle z^2\rangle) . \quad (9)$$

In calculating the reflectivity of a complex system containing many layers [see Eq. (7)], the main consequence of interface or surface roughness is to modify the intensities of the different terms. However, it is assumed in this treatment that there is no correlation between the roughness at neighboring interfaces. Furthermore, roughness at one interface will result in slight changes of phase of the neutron waves at the other interfaces which is ignored. After extensive numerical tests these effects appear to be negligible provided that the sum of the effective thicknesses of two adjacent boundary interfaces is less than half the thickness of the intervening layer.

V. RESULTS OF DATA ANALYSIS

The effective potential seen by the up and down spin neutrons as they pass through the sample are shown schematically in Fig. 7. The figure was drawn using nominal thicknesses of the individual layers in the sample as determined from thickness deposition monitors in the sputtering chamber, and values of b_i/V_i calculated using bulk densities and nominal layer compositions. The magnetic scattering length was calculated with the Permalloy magnetized in the plane of the film with 1 Bohr magneton/atom. As discussed earlier, when the Permalloy is magnetized perpendicular to the layer, the magnetic scattering goes to zero. As shown clearly by the figure, the neutrons are mostly reflected at the boundaries of the Permalloy layer. This complements the case of reflectivity of x rays from the same sample for which the strongest reflection takes place at the boundaries of the Ta layer which has the highest atomic number.

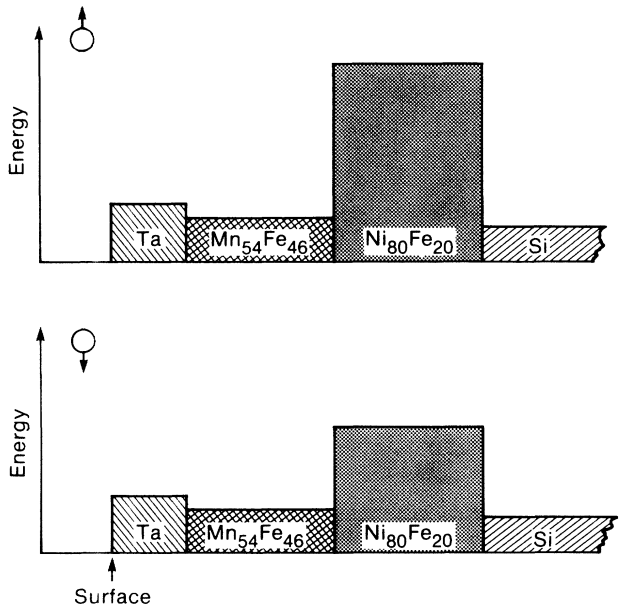

FIG. 7. Schematic diagram of the neutron potential for + and − spin neutrons through the sample.

The data was analyzed by first attempting to fit nuclear-only reflectivity data to obtain the composition profile of the sample. Using these parameters the magnetization profile was then obtained by modeling the spin-dependent reflectivities. The nuclear-only reflectivity data were obtained by placing the sample in a magnetic field of 13 kOe oriented perpendicular to the film surface. As shown in Fig. 8, the reflectivities then became spin independent with no depolarization of the neutron beam. Thus the conditions shown in Fig. 4(d) were satisfied. Initially it was attempted to use a least-squares fitting program to obtain the layer thicknesses using the nominal layer thicknesses as initial values. However, no satisfactory fits were found in this way. This might be due to the high nonlinearity of the optical transform close to the region of total reflectivity.

The well-defined minima in the reflectivity data in Fig. 8 allow an accurate determination of the thickness of the Permalloy layer. The reflectivity calculated for a single layer of Permalloy, 440 Å thick, on silicon is in good agreement with the experimental data as shown in Fig. 9(a). Although the calculated curve reproduces well the positions of the principal minima, the model is too simple to explain the secondary features in the experimental data. Obviously, we expect better agreement by including an overlayer on top of the Permalloy layer. However it was not possible to separately distinguish the Ta and Fe-Mn layers. Thus, the data were fitted by an overlayer

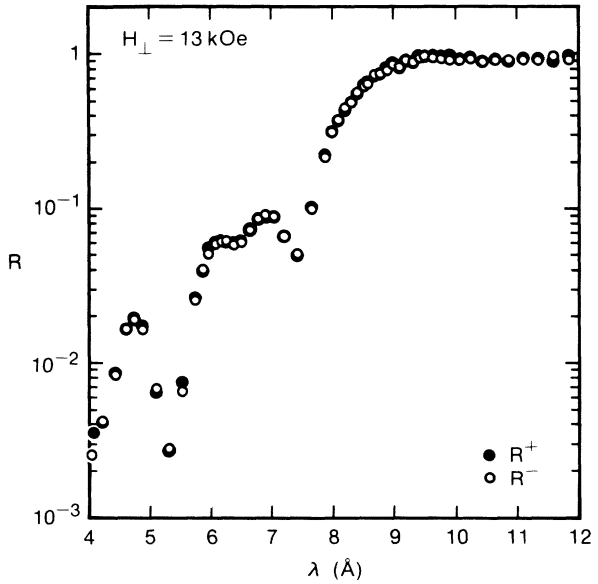

FIG. 8. + and − spin neutron reflectivities for an applied field of 13 kOe oriented perpendicular to the sample surface.

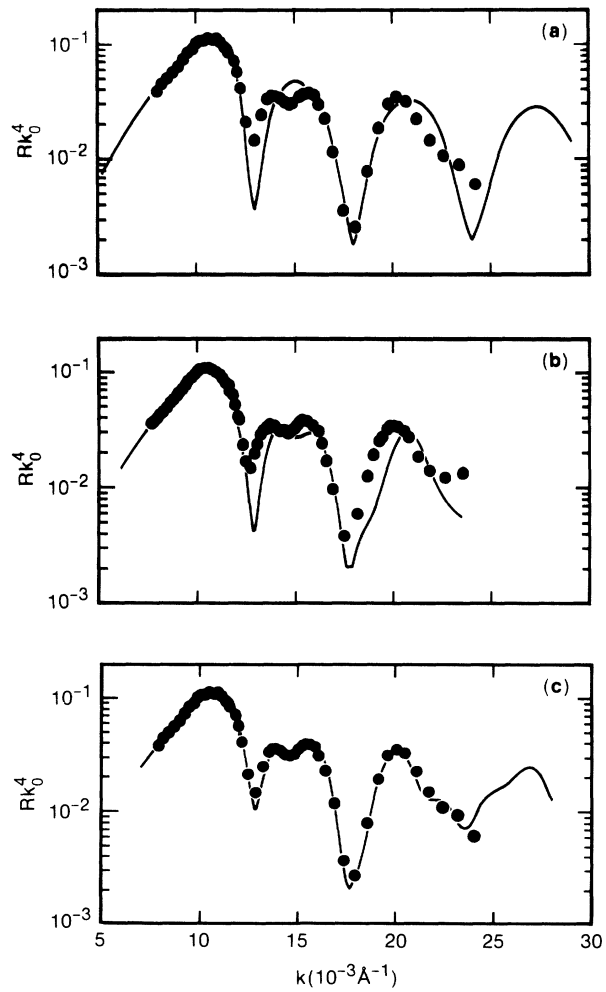

FIG. 9. Comparison of Rk_0^4 with that calculated for models of increasing complexity. Upper: one layer on silicon; middle: two layers; lower: three layers (see the text). ● average of + and − experimental reflectivities; ——: calculated reflectivity.

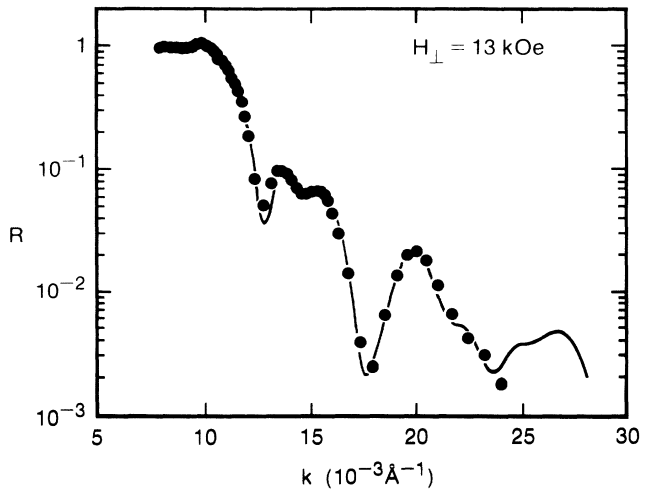

FIG. 10. Comparison of nuclear-only reflectivity with the best calculated reflectivity.

with a scattering potential set equal to the average of those for Ta and Fe-Mn. Reasonable agreement with the experimental curve was obtained for an overlayer thickness of about 600 Å, which was the nominal thickness of the combined Ta/Fe-Mn layers, although the best agreement was obtained for an overlayer 800 Å thick [Fig. 9(b)]. As discussed in detail in Sec. II, the film was analyzed in great detail using a variety of other analytical techniques. X-ray fluorescence data gave thicknesses of Ta: 335 Å, Fe-Mn: 420 Å and Ni-Fe: 400 Å, whereas RBS analysis gave Ta: 320 Å and Fe-Mn+Ni-Fe: 890 Å. Taking into account these thicknesses the best fit to the neutron data gave thicknesses of Ta: 370 Å, Fe-Mn: 460 Å, and Ni-Fe: 450 Å. These values are about 10%

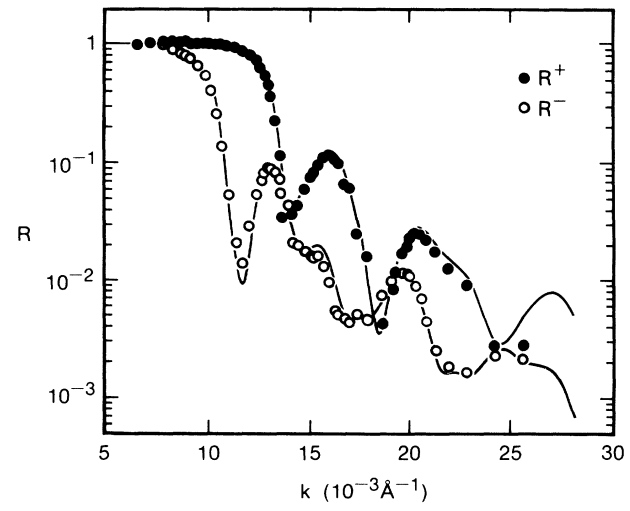

FIG. 11. Comparison of experimental (solid and open circles correspond to + and − spin) with calculated spin-dependent reflectivities for in plane applied field of 30 Oe. The chemical depth profile used was that determined from the best fit to the nuclear only reflectivity (Fig. 10). A uniform magnetization profile was used for the Permalloy layer.

higher than those given by-xray fluorescence. Excellent agreement was obtained with the experimental data using these values [see Fig. 9(c)]. The Permalloy layer thickness was determined from the neutron data with an accuracy of about ± 10 Å, but the other layer thicknesses were less well defined. The nuclear reflectivity versus k_0 is given in Fig. 10.

Experimental spin-dependent reflectivities as a function of k_0 are presented in Fig. 11. These were obtained by applying a saturating field of 30 Oe in the plane of the sample. The data were collected at various angles of incidence because of the limited range of available neutron wavelengths (4–8 Å) over which the neutron beam is sufficiently well polarized. This range is too limited to cover a broad enough k_0 region. The calculated curves (shown as solid lines in the figure) were obtained using the layer thicknesses deduced from the nuclear-only reflectivity as outlined in the preceding paragraph and a uniform magnetization of the Permalloy layer corresponding to that of bulk permalloy, $M = 823$ emu/cm^3. The agreement is quite good and further modeling shows that any non-uniformities of the Ni-Fe layer, such as "wetting" of a layer at the Ni-Fe/Fe-Mn interface, must be confined to a layer less than $\simeq 20$ Å thick. In principle, extending the measurements to higher values of k_0 should give higher resolution. However, the analysis over such short length scales imposes more and more stringent requirements on the flatness of the individual layers in the sample.

VI. CONCLUSIONS

The profile of the magnetization in the Permalloy layer of the trilayer structure, Si(111)/$Ni_{81}Fe_{19}$(400 Å)/$Fe_{50}Mn_{50}$(400 Å)/Ta(300 Å), was determined nondestructively by measuring the reflectivity at glancing incidence of (+)- and (−)-polarized neutron beams as a function of wavelength. The layer thicknesses were independently determined for the geometry in which the neutron reflectivity becomes spin independent when the magnetic moment of the structure is oriented perpendicular to the film. These results show no evidence for any deviation from a uniform magnetization distribution throughout the thickness of the Permalloy layer. Moreover, the layer-by-layer profile of the magnetization for the film saturated parallel or antiparallel to the unidirectional anisotropy direction is identical ruling out any possible magnetic domain-wall formation in this layer. Indeed these results show that the $Ni_{81}Fe_{19}/Fe_{50}Mn_{50}$ interface is magnetically abrupt within the experimental resolution of about 20 Å. While the explanation for the low values of exchange anisotropy in the $Ni_{81}Fe_{19}/Fe_{50}Mn_{50}$ remains unanswered, these results clearly establish that polarized neutron reflectometry is a powerful tool for the nondestructive examination of buried magnetic interfaces.

ACKNOWLEDGMENTS

We thank C. Corpuz and J. K. Howard for preparing the film used in this study. We also thank T. C. Huang for x-ray fluorescence measurements, G. Gorman for x-ray diffraction patterns, M. Lang and M. Toney for Auger-electron spectroscopy (AES) data, and D. Miller for x-ray photoelectron spectroscopy (XPS) data. In addition we are happy to acknowledge D. Fowler for useful discussions. This work was supported at Argonne by the U.S. Department of Energy, BES-Material Sciences, under Contract No. W-31-109-Eng-38.

[1]W. H. Meiklejohn and C. P. Bean, Phys. Rev. B **102**, 1413 (1959).

[2]L. Néel, Ann. Phys. (N.Y.) **2**, 61 (1967).

[3]A. Yelon, in *Physics of Thin Films,* edited by M. Francombe and R. Hoffmann (Academic, New York, 1971), Vol. 6, p. 205.

[4]R. D. Hempstead, S. Krongelb, and D. A. Thompson, IEEE Trans. Mag. **14**, 521 (1978).

[5]C. Tsang, N. Heiman, and K. Lee, J. Appl. Phys. **52**, 2471 (1981).

[6]C. Tsang and K. Lee, J. Appl. Phys. **53**, 2605 (1982).

[7]C. Schlenker, S. S. P. Parkin, J. C. Scott, and J. K. Howard, J. Magn. Magn. Mater. **54–57**, 801 (1986).

[8]S. S. P. Parkin, D. P. Brunco, and V. S. Speriosu, Bull. Am. Phys. Soc. **32**, 802 (1987).

[9]V. S. Speriosu, S. S. P. Parkin, and C. H. Wilts, IEEE Trans. Magn. **23**, 2999 (1987).

[10]D. Mauri, E. Kay, D. Scholl, and J. K. Howard, J. Appl. Phys. **62**, 2929 (1987).

[11]D. Mauri, H. C. Siegmann, P. S. Bagus, and E. Kay, J. Appl. Phys. **62**, 3047 (1987).

[12]W. Stoecklein, S. S. P. Parkin, and J. C. Scott, Phys. Rev. B **38**, 6847 (1988).

[13]A. P. Malozemoff, Phys. Rev. B **35**, 3679 (1987); J. Appl. Phys. **63**, 3874 (1988).

[14]G. P. Felcher, R. O. Hilleke, R. K. Crawford, J. Hanmann, R. Kleb, and G. Ostowski, Rev. Sci. Instrum. **58**, 609 (1987).

[15]S. S. P. Parkin, R. Sigsbee, R. Felici, and G. P. Felcher, Appl. Phys. Lett. **48**, 604 (1986).

[16]J. Jacobsen, *Progress in Optics,* edited by E. Wolf (North-Holland, Amsterdam, 1966).

[17]E. Hruslov, Math. USSR Sbornik **28**, 229 (1976). Note that in this treatment the potential is calculated from the reflectance of given amplitude and phase.

[18]O. S. Heavens, *Optical Properties of Thin Solid Films* (Dover, New York, 1965).

[19]J. Penfold, *Neutron Scattering at a Pulsed Source,* edited by R. J. Newport, B. Rainford, and R. Cywinski (Adam-Hilger, Bristol, 1988).

[20]B. Sheldon, J. S. Haggerty, and A. G. Emslie, J. Opt. Soc. Am. **72**, 1049 (1982).

[21]L. Nevot and P. Croc, Phys. Appl. **15**, 761 (1980).

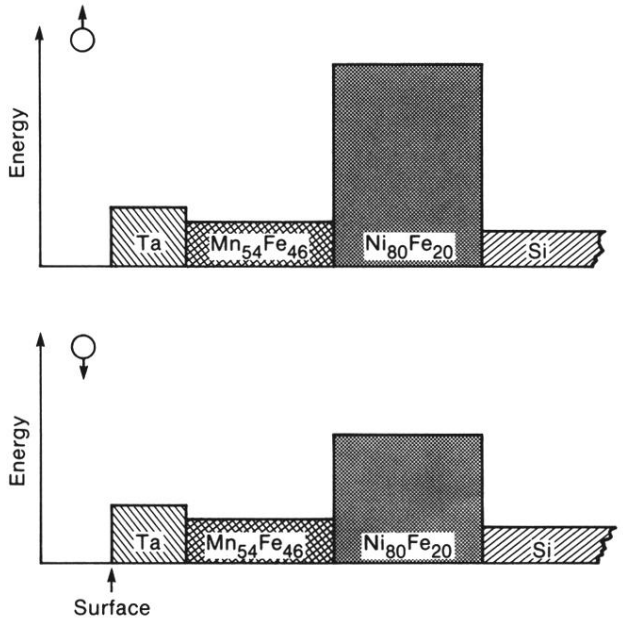

FIG. 7. Schematic diagram of the neutron potential for + and − spin neutrons through the sample.